Carbohydrate Polymers 173 (2017) 412–421

Contents lists available at ScienceDirect

Carbohydrate Polymers

journal homepage: www.elsevier.com/locate/carbpol

Ferrocene-modified chitosan as an efficient and green heterogeneous catalyst for sulfate-radical-based advanced oxidation process

Kun-Yi Andrew Lin[a,*], Jyun-Ting Lin[b], Hongta Yang[b,*]

[a] Department of Environmental Engineering, National Chung Hsing University, Taiwan
[b] Department of Chemical Engineering, National Chung Hsing University, 250 Kuo- Kuang Road, Taichung, Taiwan

ARTICLE INFO

Article history:
Received 12 January 2017
Received in revised form 25 April 2017
Accepted 5 June 2017
Available online 6 June 2017

Keywords:
Ferrocene
Chitosan
Amaranth
Persulfate
EPR
AOPs

ABSTRACT

While ferrocene (Fc) is a promising heterogeneous catalyst for activating persulfate (PS) to degrade organic contaminants, chemical reagent-grade Fc is nanoscale and direct usage of Fc leads to operational and recovery issues. In this study, chitosan (CS) is selected as a support to immobilize Fc as CS is abundant, and environmental benign fishery waste. The amine group of CS also allows the formation of covalent bond between Fc-based reagent (*i.e.*, Fc-CHO) and CS to form Fc-modified CS (Fc-CS). This Fc-CS can be more advantageous than Fc because of its easier recovery by precipitation and filtration. To evaluate Fc-CS for PS activation, degradation of Amaranth (AMR) dye by PS is selected as a model test. The resulting Fc-CS exhibits a higher catalytic activity than pristine Fc possibly because Fc can be evenly dispersed on CS and CS can also exhibit affinity toward AMR. AMR can be also fully decomposed by Fc-CS activated PS. Through the Electron paramagnetic resonance (EPR) spectroscopic analysis, the AMR degradation can be attributed to both sulfate and hydroxyl radicals. Fc-CS had been also proven to activate PS for AMR degradation over multiple times without loss of catalytic activity. These features indicate that Fc-CS can be a promising catalyst and CS appears to be a naturally available and environmentally friendly waste-derived support for immobilizing Fc. The results and findings in this study are essential for CS-supported metal catalysts in environmental applications.

1. Introduction

Chemical oxidation is considered as the most effective and rapid approach to treat organic pollutants in wastewater treatments. Techniques of chemical oxidation are typically categorized as advanced oxidation processes (AOPs), in which high-oxidation-potential radical species, such as hydroxyl ($OH^{\bullet}$) and sulfate ($SO_4^{\bullet-}$) radicals, are obtained from oxidants for degrading organic contaminants. Despite the fact that $OH^{\bullet}$-involved AOPs (*e.g.*, Fenton's reaction) have been well established and employed widely (Liao, Sun, & Gao, 2009), $SO_4^{\bullet-}$-involved AOPs also receive increasing attention because $SO_4^{\bullet-}$ exhibits a high degradation selectivity towards aromatic/unsaturated chemical structures with a relatively short half-life compared to $OH^{\bullet}$ (Neta, Huie, & Ross, 1988).

To obtain $SO_4^{\bullet-}$, persulfate (PS) represents as the most extensively used oxidant because PS is commercially available, inexpensive, and environmentally friendly (Hu & Long, 2016; Zhao, Yeung, & Dong, 2010). Therefore, PS has been favorably employed in many chemically oxidative applications, including cleaning (King, 1983; Kiener, 1991), disinfecting (Ahn, Peterson, Righter, Miles, & Tratnyek, 2013), and environmental remediation (Hu & Long, 2016; Liang, Bruell, Marley, & Sperry, 2004; Lin, Chang, & Hsu, 2015; Matzek & Carter, 2016). Nevertheless, proper activation of PS is required to generate $SO_4^{\bullet-}$ more efficiently (Matzek & Carter, 2016; Yang et al., 2010). To do so, several techniques have been developed to activate PS such as heating (Huang, Couttenye, & Hoag, 2002; Yang et al., 2010), light irradiation (Gao, Gao, Deng, Yang, & Ma, 2012; Yang et al., 2010), ultrasonication (Kurukutla, Kumar, Anandan, & Sivasankar, 2014) and catalysts (Lu, Wang, Xu, Liu, & Qian, 2016; Lin, Lin, & Jochems, 2017; Weng & Tao). Even though heating, light and sonication can successfully activate PS, these techniques require continuous energy consumption. Therefore, activation of PS by catalysts is considered as a relatively practical technique (Matzek & Carter, 2016).

To date, many metals are proven to activate PS, such as iron (Cai, Zhang, & Zhang, 2016; Liang, Liang, & Chen, 2009; Liu et al., 2016; Wu et al., 2017), cobalt (Zhang, Chen, & Zhu, 2016), manganese (Liu et al., 2016), copper (Liu, Shih, Sun, & Wang, 2012; Zeng et al., 2016), etc. Among these metals, Fe has been recognized as the most effi-

* Corresponding authors.
E-mail addresses: linky@nchu.edu.tw (K.-Y.A. Lin), hyang@nchu.edu.tw (H. Yang).

http://dx.doi.org/10.1016/j.carbpol.2017.06.015
0144-8617/

cient catalyst for PS activation (Matzek & Carter, 2016). However, the direct addition of Fe ions can cause environmental problems if these metals are not recovered; therefore heterogeneous Fe-containing materials appear to be more advantageous. However, turning Fe ions into solid Fe-containing materials typically involves complicated procedures and relatively long preparation time (Lu et al., 2016). Therefore, if there is a Fe-containing solid compound, which is readily available, easily accessible, and highly stable in water, this type of compound would be a suitable catalyst for PS activation. Herein, ferrocene (Fc), which is comprised of a central Fe^{2+} bound by two cyclopentadienyl rings, appears to be a promising candidate meeting the aforementioned requirements. Fc has been validated as a highly stable and non-toxic compound (Nie, Hu, Qu, & Hu, 2008; Wang, Tian, Cun, & Ning, 2013), and it can exhibit excellent redox reversible properties (Li et al., 2009; Tsai, Chang, Liu, Chen, & Jenekhe, 2005; Wang et al., 2013). Therefore, Fc is proposed as a heterogeneous catalyst to activate various oxidants (Lin et al., 2017; Nie et al., 2008; Wang et al., 2013; Ye, Cui, & Wang, 2014).

Nevertheless, since chemical reagent-grade Fc in fact is a nanoscale material (Lin et al., 2017), it is impractical to use Fc directly in view of operational and recovery issues. Therefore, immobilization of Fc onto relatively large supports seems a more feasible strategy to utilize Fc because the supported Fc can be easily collected by precipitation or filtration. In addition, the supported Fc can be even packed into columns for continuous operations. However, the immobilization process of Fc onto supports should be straightforward and supports must be environmentally benign at very low cost. To this end, chitosan (CS) seems an ideal support because CS can be derived from abundant fishery wastes and CS consists of primary amine groups, which can be utilized to make bonds with Fc-related compounds. The resulting Fc-chitosan (Fc-CS) composite can be a practical and green heterogeneous catalyst for PS activation. Nevertheless, to our knowledge, no studies have been conducted to investigate this Fc-CS material and its potential for PS activation.

To evaluate Fc-CS for PS activation, degradation of Amaranth (AMR) dye by PS is selected as a model test. PS activation behaviors by Fc-CS are thoroughly investigated by examining various effects on AMR degradation, including dosages of Fc-CS and PS, temperature, initial pH, and co-existing compounds. Electron paramagnetic resonance (EPR) spectroscopy is adopted to determine radical species generated during PS activation by Fc-CS (Fc-CS + PS) to study mechanisms of PS activation by Fc-CS and AMR degradation. The recyclability of Fc-CS for activating PS is also demonstrated to reveal its long-term re-usability.

2. Experimental

2.1. Preparation and characterization of fc-CS

Chemicals involved in this study were commercially available and used as received without additional purification. The preparation scheme for Fc-CS can be illustrated in Fig. 1(a). In this study, ferrocenecarboxaldehyde (Fc-CHO) (98%, Sigma Aldrich, USA), is selected as an Fc-bearing compound because the CHO group of Fc-CHO can react with the NH_2 group of CS via a Schiff-based reaction to form a covalent bond (*i.e.*, −C═N−) (Ye, Cui et al., 2014; Ye, Zheng, & Wang, 2014). In brief, the as-received CS (Sigma-Aldrich, USA, practical grade derived from shrimp shells; MW: 190K–375 K Da; deacetylation degree ≥75%). Subsequently, 1 g of CS powder was added to 100 mL of anhydrous ethanol to prepare an ethanolic CS suspension. Fc-CHO (0.25 g) (Sigma-Aldrich, 98%, USA) was then gradually added to the suspension, and the resulting mixture was stirred under nitrogen atmosphere at 100 °C for 12 h. The Fc-modified CS was then collected and washed repeatedly with ethanol and deionized (DI) water, and dried at 60 °C for 24 h to yield the final product, Fc-CS. To study the effect of Fc content in Fc-CS on PS activation for AMR degradation, various dosages of Fc-CHO were used to prepare Fc-CS for obtaining Fc-CS with Fc contents ranging from 0.7 to 6.4 wt%.

The as-prepared Fc-CS was first characterized using scanning electronic microscopy (JEOL JSM-6700, Japan) with energy dispersive X-ray spectrometer (EDS) (Oxford Instruments, UK) to reveal its morphology and chemical composition. The XRD pattern of Fc-CS was measured by an X-ray diffractometer (Bruker, USA). The surface chemistry of Fc-CS was determined by an X-ray photoelectron spectroscopy (XPS) (PHI 5000 ULVAC-PHI, Japan). Thermogravimetric (TG) analysis of Fc-CS was performed using a TG analyzer (ISI i1000, USA) in N_2. The light absorption properties of Fc-CS, CS and Fc were obtained using a UV–vis spectrophotometer equipped with integrating spheres (V650 Jasco, Japan) to collect diffuse reflectance spectrum.

2.2. Activation of PS by fc-CS for degradation of AMR

Activation of PS by Fc-CS was studied by batch-type experiments of AMR degradation. AMR was particularly selected because it is extensively employed in textile and even added to foods as food colorants (Gupta et al., 2012; Sudrajat & Babel, 2015), but AMR has been validated to cause allergic and respiratory problems (Mittal, Kurup, & Gupta, 2005) and tumors in animals (Chung, Fulk, & Egan, 1978). Thus, it is necessary to degrade AMR to prevent its negative environmental and healthy impact.

In a typical experiment, a certain amount of Fc-CS (*e.g.*, 50 mg) was added to a glass batch reactor containing 200 mL of AMR solution (Sigma-Aldrich, 95%, USA) with an initial concentration (C_0) of 50 mg L^{-1}. While the AMR solution was stirred (200 rpm) and maintained at a desired temperature, a given dosage of PS (40 mg) (Alfa Aesar, 98%, USA) was immediately added. At pre-set times, sample aliquots were taken from the mixture and Fc-CS was immediately separated from the AMR solution by filtration. The residual concentration of AMR in sample aliquots was determined by a UV–vis spectrophotometer (Chrom-Tech CT-2000, Taiwan) at 520 nm.

The effect of temperature on activation of PS for AMR degradation was examined by changing temperature to 30, 40 and 50 °C. The initial pH of AMR solution was also investigated by adjusting pH to 3, 5, 9, and 11 using 0.1 M of HNO_3 and NaOH. As wastewater typically consists of various compounds, the presence of surfactants may also affect the PS activation. Thus, an anionic surfactant, sodium dodecyl sulfate (SDS), and a cationic surfactant, cetyltrimethylammonium bromide (CTAB), were selected for evaluating the influence of surfactants (50 mg L^{-1}). The effect of salt was also examined by adding NaCl (50 mg L^{-1}) during AMR degradation. To further determine the degradation mechanism by PS activation using Fc-CS, EPR spectroscopy (Bruker EPR spectrometer (EMX-P)) with 5,5-Dimethyl-1-pyrroline N-oxide (DMPO) as a radical-trapping agent was employed to measure radical species during PS activation by Fc-CS. The recyclability of Fc-CS for activating PS to degrade AMR was evaluated by re-using Fc-CS for activating PS over multiple times without regeneration treatments. When AMR degradation by Fc-CS-PS was completed, Fc-CS was recovered by centrifugation, washed with DI water and dried at 65 °C. The recovered Fc-CS was then added to another batch of AMR degradation experiment. The recovered Fc-CS was then used to activate PS for another batch of AMR degradation. Since the AMR degradation was a batch experiment, Fc-CS remained in the solution and only a small amount of Fc-CS was taken out because of sampling withdrawal. We did do mass balance of Fc-CS to calculate Fc-CS remained in the solution and taken out by sampling. We found that total weight of Fc-CS remained quite comparable with a

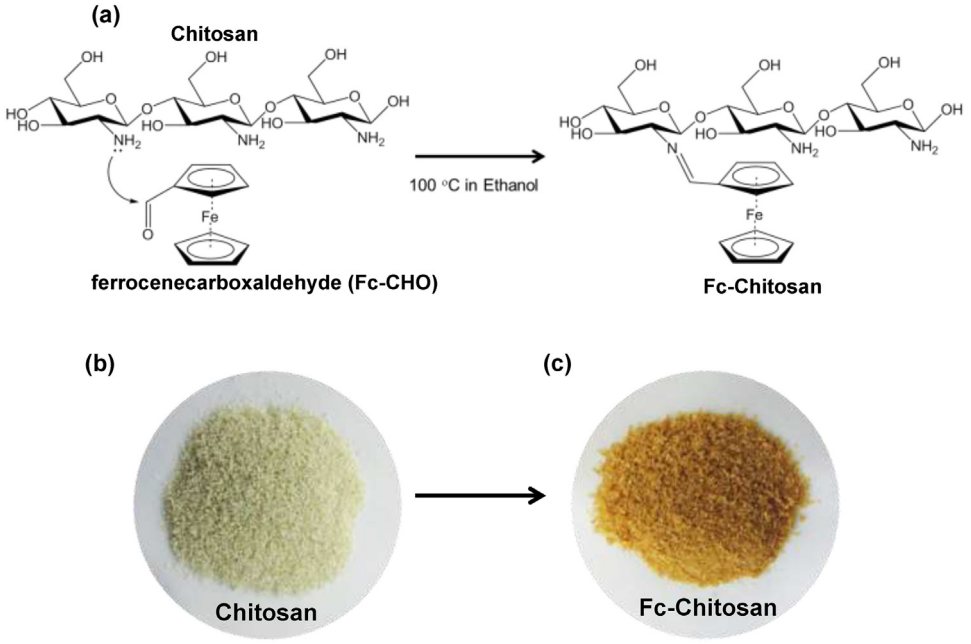

Fig. 1. Fc-chitosan: (a) preparation scheme; images of (b) the unmodified chitosan and (c) Fc-chitosan.

slight change less than 3 wt%. This was probably that Fc-CS in fact was a powder-like bulky material and could be easily collected by filtration or centrifugation.

3. Results and discussion

3.1. Characterizations of fc-CS

The modification of CS by Fc can be visualized in Fig. 1(b) and (c). Fig. 1(b) shows the pristine CS powder which exhibits a typical light-yellow color of CS. The color of CS changed to brown after CS was modified by dark brown-colored Fc-CHO (Fig. 1(c)). The color change of CS by Fc-modification can be further validated using diffuse reflection spectroscopy which displays light absorption properties of solid materials. Fig. S1(a) reveals that Fc can absorb a relatively wide range of visible light up to *ca.* 550 nm owing to its dark-brown color, whereas the dominant light absorption range of CS is up to *ca.* 450 nm. After CS was modified by Fc, the resulting Fc-CS exhibited a much wider range of light absorption extending to 550 nm in comparison with CS. This confirms that Fc was immobilized on the CS surface and made the color of CS changed.

Fig. 2(a) further reveals a microscopic image of Fc-CS, which shows a plaque-like morphology with quite smooth surfaces. A closer view of Fc-CS (Fig. 2(b)) shows that the surface of Fc-CS exhibited fibrous configurations and some pores existed. As CS powder was quite large (≥100 μm) with a certain thickness (a few μm), Fc was expected to modify the CS surface only. For comparison, images of pristine CS are also provided in Fig. S2; pristine CS exhibits also smooth but fibrous structures. This indicates that the morphology of CS remained similar even after the Fc modification. Elemental compositions of Fc-CS were analyzed using EDS during SEM measurements (Fig. 2(c)). In comparison with the pristine CS, there are a few additional peaks in the spectrum of Fc-CS at 0.7 and 6.4 KeV, attributed to Fe, indicating that Fc was incorporated into CS.

Fig. 3 further reveals distributions of elemental species in Fc-CS. As CS is comprised of C, N and O, these elements are abundant and evenly distributed on Fc-CS. In addition, Fe can be also detected on the surface of Fc-CS, confirming that Fc was certainly grafted to CS. On the other hand, since Fe was also evenly distributed on CS without aggregation, the graft of Fc to CS was considered to occur via a specific reaction, which is the nucleophilic addition of NH_2 with aldehydes owing the aforementioned Schiff base reaction.

The XRD pattern of Fc-CS is displayed in Fig. 2(d), in which two broad peaks can be observed at $2\theta = 10$ and 20° (Abdeen, Mohammad, & Mahmoud, 2015; Chen, Xu, Li, Wang, & Zhang, 2011). As these two peaks are the characteristic peaks of pristine CS (Fig. S3), the XRD pattern of Fc-CS indicates that the XRD pattern of CS remained the same after the Fc-modification. In addition, the surface chemistry of Fc-CS is further revealed by the XPS analysis in Fig. 4(a), confirming that Fc-CS was comprised of C, N, O and Fe. Fig. 4(b) further shows the C1 s core-level spectrum, which can be deconvoluted to exhibit two peaks at 285.0 and 286.7 eV, corresponding to the C—C and C—O bond, respectively. On the other hand, the core-level spectrum of N1 s can be seen in Fig. 4(c); the single peak at 400 eV can be assigned to the unreacted N—H bond of the primary amine in CS (Liu, Zhang, Wang, Dawson, & Chen, 2011). The F2p core-level spectrum shown in Fig. 4(d) can be also deconvoluted to several peaks. In particular, the tall peaks at 710.0, and 723.8 eV, which are attributed to $F2p_{3/2}$, and $F2p_{1/3}$ peaks of Fe^{2+}, respectively (Lin et al., 2017). As Fe in Fc exists in the form of Fe^{2+}, the existence of Fe^{2+} in Fc-CS ascertains the incorporation of Fc into CS and its valence state remains unchanged after the modification.

TGA analysis of Fc-CS is shown in Fig. S4, in which TG data of Fc and CS are also displayed. Pristine CS exhibited a small weight loss starting from 30 to 100 °C, due to evaporation of moisture, followed by a huge weight loss at 250 °C due to its decomposition. On the other hand, Fc was rapidly decomposed starting from 90 °C. The TG curve of Fc-CS was quite similar to that of pristine CS except that the weight loss occurred around 100 oC was much more, due to the decomposition of Fc. The difference between these TG curves suggests the fraction of Fc in Fc-CS, which was estimated to 6.4 wt%.

3.2. Activation of PS by fc-CS for AMR degradation

Before evaluating PS activation by Fc-CS, it is important to ensure whether Fc-CS can decolorize AMR via adsorption. Fig. 5(a) reveals that Fc-CS slightly decolorized AMR as C_t/C_0 approached

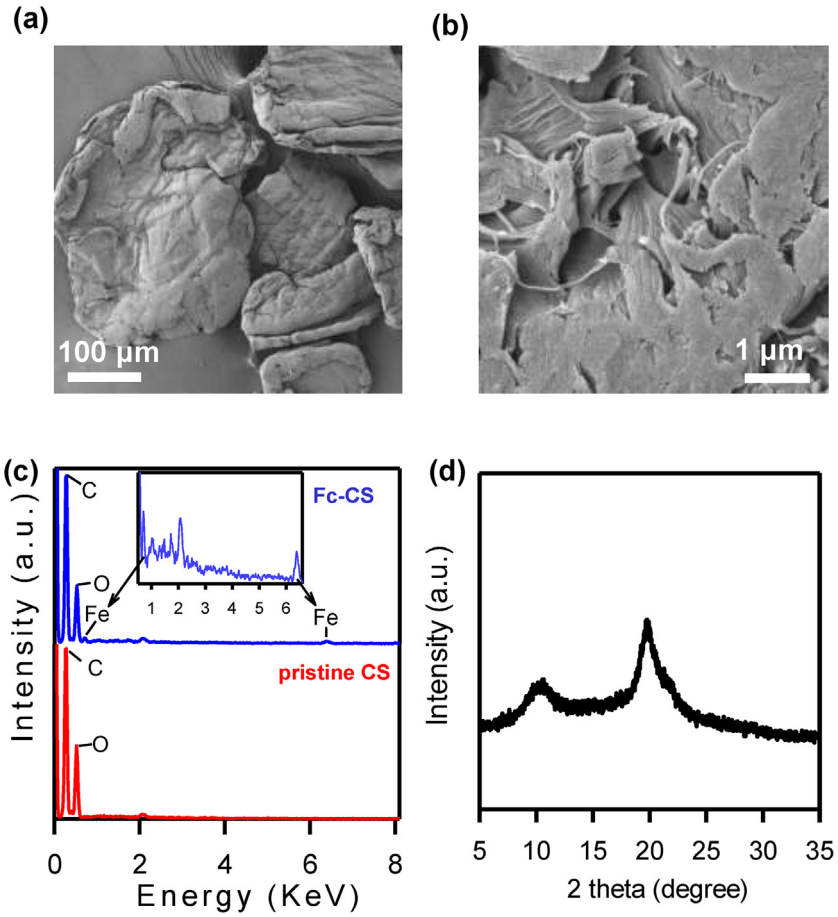

Fig. 2. Characterization of Fc-CS: (a) and (b) SEM images at different magnifications; (c) EDS spectrum and (d) XRD pattern.

0.95 after 120 min. Since AMR is an anionic dye, AMR could be attracted to Fc-CS because CS consists of amine groups. On the other hand, PS was also evaluated for AMR degradation, and PS alone also slightly degraded AMR. However C_t/C_0 at 120 only reached 0.92, demonstrating that PS was inefficient for AMR degradation without activation. Once PS was combined with Fc-CS, AMR was quickly degraded and C_t/C_0 approached zero after 90 min. As PS and Fc-CS both were ineffective individually for AMR degradation, this result suggests that PS was certainly activated in the presence of Fc-CS.

As revealed in the XPS result, Fc-CS was comprised of Fe^{2+} derived from Fc,

Fe^{2+} is considered to activate PS for generating sulfate radicals as follows (Eq. (1)) (Rodriguez, Vasquez, Costa, Romero, & Santos, 2014; Zhao et al., 2013):

$$Fe^{2+} + S_2O_8{}^{2-} \rightarrow Fe^{3+} + SO_4{}^{\bullet -} + SO_4{}^{2-} \quad (1)$$

The oxidized state of Fe^{3+} can be reduced to Fe^{2+} in contact with another PS molecule as follows (Eq. (2))(Liu, Bruton, Doyle, & Sedlak, 2014; McElroy & Waygood, 1990; Yu, Bao, & Barker, 2003).

$$Fe^{3+} + S_2O_8{}^{2-} \rightarrow Fe^{2+} + S_2O_8{}^{\bullet -} \quad (2)$$

These high-oxidation-potential radicals attacked AMR and then decomposed AMR. While the activation capability of Fc-CS was attributed to Fc, it is interesting to compare AMR degradation of Fc-CS with Fc. Fig. 5(a) displays that when pristine Fc (250 mg L^{-1}) was used to activate PS, Fc indeed activated PS and caused decomposition of AMR rapidly as C_t/C_0 approached to zero after 60 min. To quantitatively compare kinetics, the apparent pseudo first order rate law is thus employed by the following equation (Eq. (3)):

$$C_t = C_0 \exp(-k_{app} t) \quad (3)$$

where k_{app} is the apparent pseudo first order rate constant for AMR degradation. The k_{app} values for AMR degradation under various conditions are listed in Table S1 (see the supporting information). Although Fc-CS (k_{app} = 0.026 min^{-1}) appeared to be slower than Fc (k_{app} = 0.088 min^{-1}) for activating PS, the fraction of Fc in Fc-CS was only 6.4 wt% and AMR degradation can be still completed by Fc-CS + PS. Furthermore, we also found that if an equivalent amount of Fc in Fc-CS (*i.e.*, 16 mg L^{-1}) was added to activate PS, the corresponding AMR degradation (k_{app} = 0.017 min^{-1}) was not as effective as that by Fc-CS + PS. This result suggests that when a certain amount of Fc is immobilized onto CS, the resulting Fc-CS composite can be more advantageous than the same amount of Fc for activating PS. This might be because Fc was quite evenly distributed on the CS surface without aggregation (as shown in Fig. 3) and Fc-CS was dispersed in water with stirring. Thus, these Fc moieties present on the CS surface should remain highly accessible to PS to initiate the activation. In addition, the CS matrix, which contains amine functional groups, exhibits affinities toward AMR and then attracts AMR. Thus, approach of AMR to the surface of Fc-CS, where sulfate radicals were formed, was facilitated, leading to the improved AMR degradation.

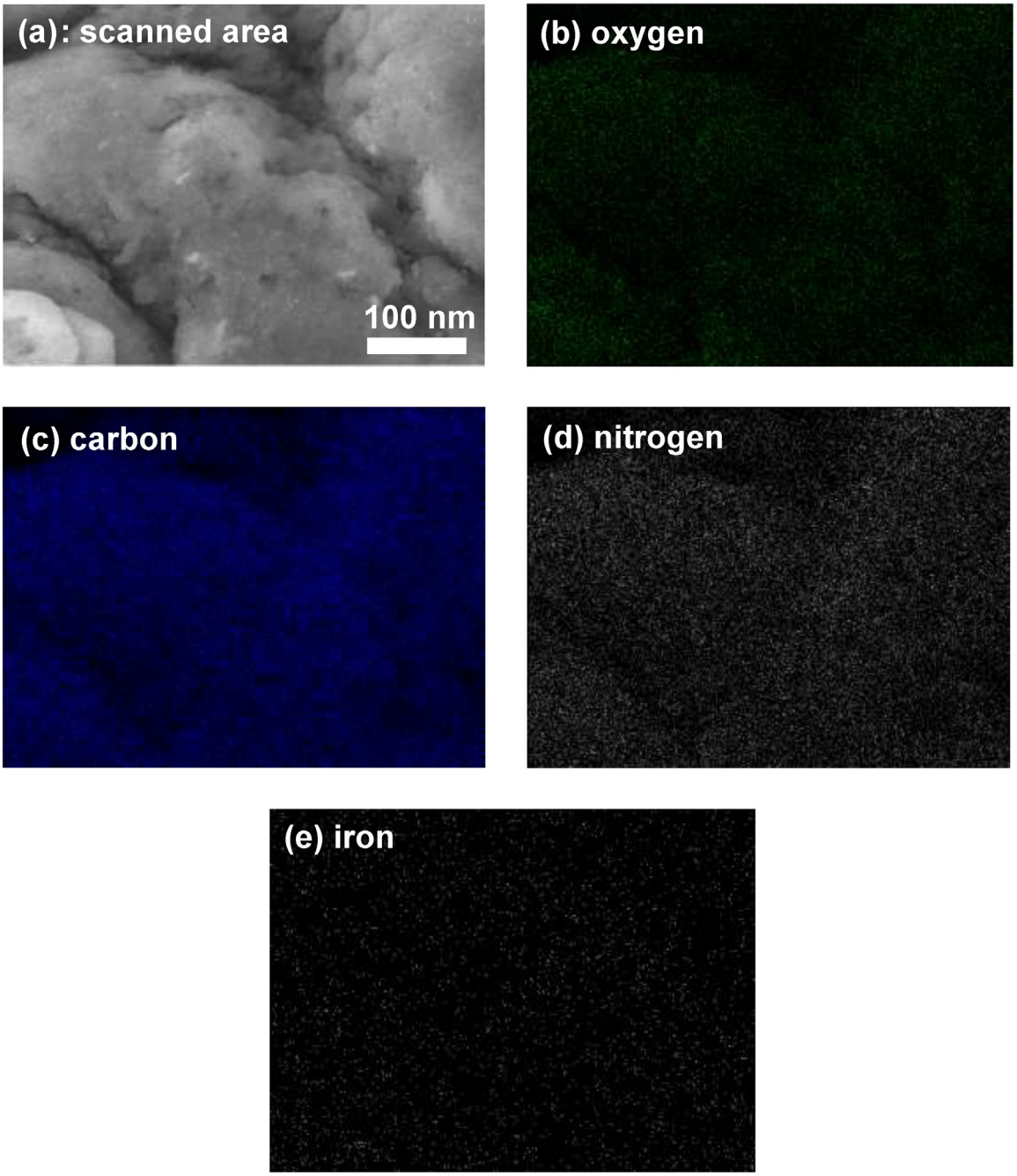

Fig. 3. Mapping results of constituent elements of Fc-CS: (a) the scanned area, (b) oxygen, (c) carbon and (d) iron.

3.3. Effects of Fc-CS, PS dosage and Fc content on PS activation for AMR degradation

While Fc-CS can activate PS, it is essential to investigate the respective effects on PS activation for AMR degradation. Fig. 5(b) shows the effect of Fc-CS dosage varied from 125 to 500 mg L^{-1} on AMR degradation. One can note that the increase in Fc-CS from 125 to 500 mg L^{-1} certainly accelerated AMR degradation as k_{app} changed from 0.008 to 0.043 min^{-1}. This demonstrates that a higher dosage of Fc-CS facilitated PS activation and also the affinity between AMR and Fc-CS is expected to be stronger, resulting in the faster kinetics.

On the other hand, the effect of PS dosage can be seen in Fig. 6(a). While a relatively low PS dosage (100 mg L^{-1}) was present, the AMR degradation became slow and incomplete as C_t/C_0 only approached 0.3 with k_{app} = 0.011 min^{-1}. As PS dosage increased to 200 and 400 mg L^{-1}, AMR was fully degraded and k_{app} also rose to 0.026 and 0.039 min^{-1}, indicating that the PS dosage critically influenced degradation extent.

In addition, Fc content was also varied from 0.7 to 6.4 wt% by adding different Fc-CHO during Fc-CS preparation to study the effect of Fc content of Fc-CS. Fig. S5 shows that when Fc content was 0.7 wt%, AMR was also degraded as Ct/C0 reached 0.3 in 120 min. Even though Fc content was as low as 0.7 wt%, Fc-CS was still capable of activating PS for AMR degradation, validating the catalytic role of Fc. When Fc content increased to 3.8%, the degradation extent and kinetics were both improved substantially. The enhancement became even more pronounced at even higher Fc

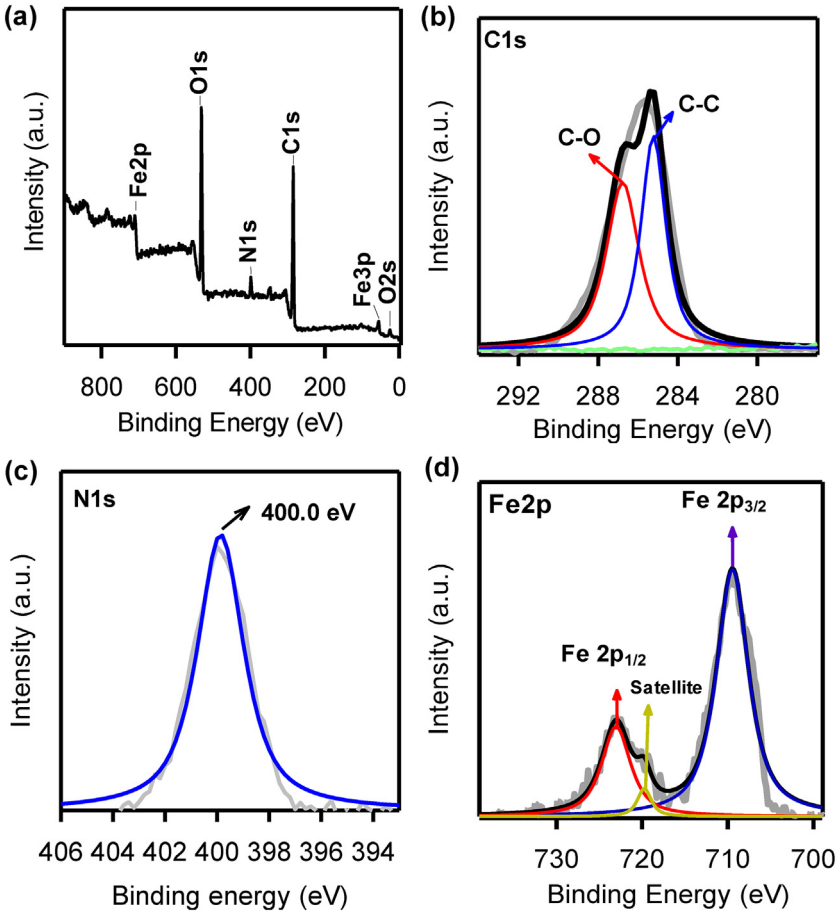

Fig. 4. Chemical analysis of Fc-chitosan by XPS: (a) full-survey spectrum, (b) C1 s core-level spectrum, (c) N1 s core-level spectrum and (d) Fe2p core-level spectrum.

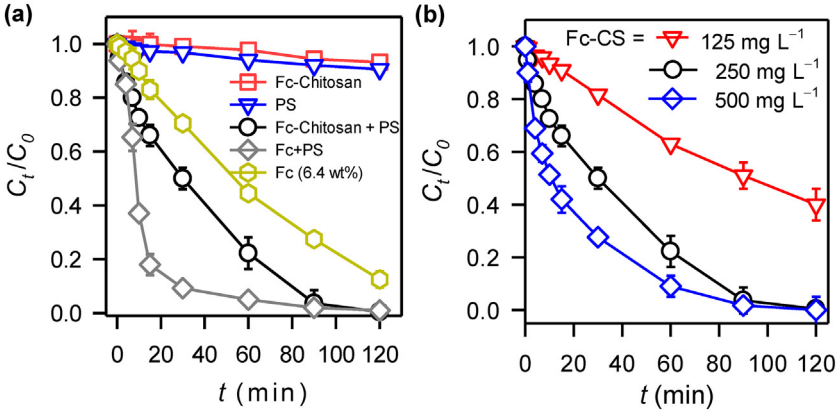

Fig. 5. AMR degradation by Fc-CS + PS: (a) a comparison between Fc-CS + PS, PS alone, Fc + PS, Fc + PS with an equivalent concentration to Fc in Fc-chitosan, adsorption to Fc-CS (Fc-CS = Fc = 250 mg L^{-1}; PS = 200 mg L^{-1}; T = 40 °C; pH = 7); (b) effect of Fc-CS dosage on activation of PS for AMR degradation (PS = 200 mg L^{-1}; T = 40 °C; pH = 7).

contents in Fc-CS (*i.e.*, 4.8 and 6.4 wt%), confirming that PS activation can be also improved by a higher loading of Fc in CS.

3.4. Effects of temperature and pH on AMR degradation

As temperature is an essential parameter for PS activation, we further evaluated the effect of temperature by changing temperature to 30, 40 and 50 °C. Fig. 6(b) shows that the temperature influenced AMR degradation and kinetics significantly. Especially, when temperature was lowered from 40 to 30 °C, AMR degradation became incomplete and k_{app} decreased from 0.026 to 0.005 min^{-1}. In contrast, k_{app} increased to 0.070 min^{-1} once temperature was raised to 50 °C, indicating that the PS activation by Fc-CS was much enhanced and facilitated at elevated temperatures.

As k_{app} increases with the increasing temperature, k_{app} may be associated with temperature by the Arrhenius equation as follows (Eq. (4)):

$$\ln k_{app} = \ln k - E_a/RT \quad (4)$$

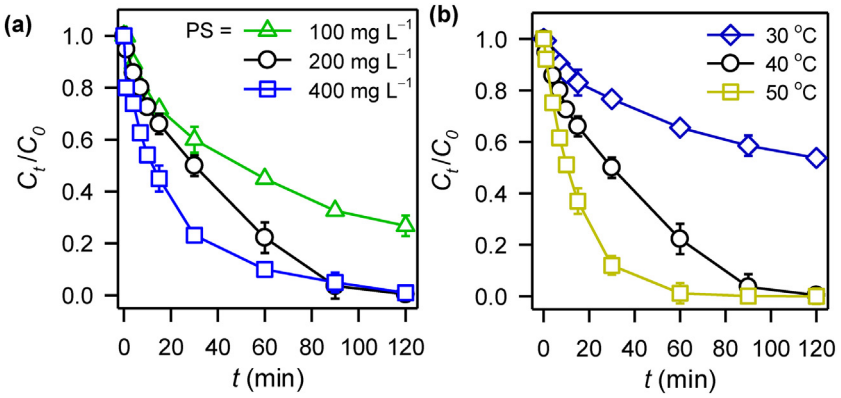

Fig. 6. AMR degradation by Fc-CS + PS: effects of (a) PS dosage (Fc-CS = 250 mg L^{-1}; T = 40 °C; pH = 7) and (b) temperature on AMR degradation by Fc-CS + PS (Fc-CS = 250 mg L^{-1}; PS = 200 mg L^{-1}; pH = 7).

where k denotes the pre-exponential factor (min^{-1}); R represents the universal gas constant; and T means temperature (K). According to Eq. (4), a plot of $1/T$ versus Ln k_{app} is displayed in Fig. S6, in which the data points can be well fit by the linear regression line (R^2 = 0.996). This indicates that the k_{app} can be appropriately associated with temperature via the Arrhenius equation for predicting k_{app} at other temperatures.

On the other hand, initial pH of solution also plays an important role in PS activation and the effect of pH was thus investigated in Fig. 7(a). In comparison with the AMR degradation without pH adjustment (*i.e.*, pH = 7), AMR degradation extents and kinetics were substantially improved at pH = 5 and even further enhanced at pH = 3. On the contrary, when pH was raised to 9 and 11, AMR degradation became less effective. These results demonstrate that the acidic conditions can facilitate AMR degradation by Fc-CS + PS, whereas the basic conditions were unfavorable for Fc-CS + PS. This could be because PS is an acidic oxidant and therefore the generation of $SO_4^{\bullet -}$ could be also accelerated at low pH (Qi, Chu, & Xu, 2014). Nevertheless, PS is prone to decompose without the generation of sulfate radicals under basic conditions (Guo, Su, Yi, & Ma, 2013; Khan & Jhung, 2009; Rastogi, Al-Abed, & Dionysiou, 2009). As a result, AMR degradation was greatly suppressed at relatively high pH values. Another possibility for the enhanced AMR degradation under acidic conditions might be because H^+ accumulated on the surface of Fc-CS at low pH. The attraction of the anionic AMR to Fc-CS became stronger and therefore facilitated AMR degradation. In contrast, the surface of Fc-CS was deposited with more hydroxyl ions (OH^-), which increased the electrostatic repulsion between AMR and Fc-CS, inhibiting AMR degradation.

3.5. Effects of co-existing compounds on AMR Degradation by Fc-CS + PS

Even though Fc-CS can activate PS for AMR degradation, other compounds existing in AMR solutions may interfere with the activation and then degradation especially in view of complex matrices in wastewater. Herein, we particularly evaluated effects of several typical co-existing compounds including salts and surfactants, which are easily detected in wastewater. We first evaluated the addition of NaCl as a representative salt as NaCl is commonly used to enhance dye-fixation during dyeing processes (Adil, Qadir, & Mahmood, 2009; Muthukumar, Sargunamani, Selvakumar, & Nedumaran, 2004; Xiang et al., 2003). Fig. 7(b) shows that the degradation extent and kinetics remained similar to those in the absence of NaCl (k_{app} = 0.026 min^{-1}), suggesting that an equivalent concentration of NaCl (*i.e.*, 50 mg L^{-1}) did not noticeably influence PS activation by Fc-CS.

On the other hand, the effects of surfactants were examined by selecting CTAB as a model cationic surfactant and SDS as a common anionic surfactant. The presence of these surfactants caused significant influences on AMR degradation extent and kinetics. The presence of CTAB, surprisingly and significantly, improved AMR degradation (k_{app} = 0.955), whereas AMR degradation was slightly suppressed in the presence of SDS (k_{app} = 0.012 min^{-1}). As these surfactants are charged, these features could be highly involved with electrostatic interactions between AMR and Fc-CS in the presence of these surfactants. One speculation is that the positively charged CTAB might reside on the surface of Fc-CS and enable Fc-CS to attract more AMR molecules, thereby facilitating the elimination of AMR. However, this process might be associated with not

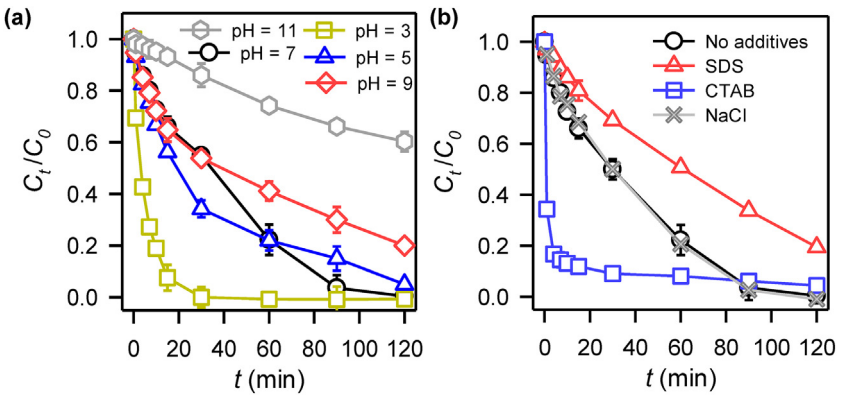

Fig. 7. Effects of (a) pH and (b) NaCl/surfactants on AMR degradation by Fc-CS + PS (Fc-CS = 250 mg L^{-1}; PS = 200 mg L^{-1}; T = 40 °C; NaCl/surfactant = 50 mg L^{-1}).

only degradation but also adsorption. By contrast, the anionic SDS present on the surface of Fc-CS might repel the approach of AMR and thus hinder the interaction between AMR and Fc-CS. These results suggest that even though wastewater is comprised of complex constituents, these co-existing compounds are not necessarily adverse to the removal of AMR.

3.6. EPR analysis and proposed mechanisms

In the earlier section, we have attributed the PS activation by Fc-CS to Fe^{2+} of Fc, which could react with PS to generate sulfate and persulfate radicals for attacking AMR. To further verify this reaction, EPR analysis was adopted to determine the radical species generated during Fc-CS + PS. Fig. 8 displays EPR spectra of Fc-CS, PS and Fc-CS + S; almost no strong signals can be detected in the cases of Fc-CS and PS alone. This validates that Fc-CS itself could not generate radicals and PS, without activation, was unable to produce radicals efficiently. Nevertheless, significant peaks were detected in the spectrum of Fc-CS + PS. Since the radical-trapping reagent used in this study was "DMPO", the four relatively tall peaks (labelled with the hollow circles) can be attributed to DMPO hydroxyl radical adduct (*i.e.*, DMPO-OH) according to literatures. The presence of DMPO-OH indicates that OH• was present and derived from $SO_4^{\bullet-}$. On the other hand, the relatively short peaks (labelled with the hollow rectangles) can be attributed to DMPO sulfate radical adduct (Yin, Hu, Song, Liu, & Lin, 2016; Zhang et al., 2016) (*i.e.*, DMPO-SO_4), confirming that sulfate radicals were produced and derived from activation of PS. This confirms that sulfate radicals were produced from Fc-CS + PS as a result of PS activation by Fc-CS. In addition, hydroxyl radicals could be also derived during Fc-CS + PS. This is because sulfate radicals ($SO_4^{\bullet-}$) is reported to react with water,

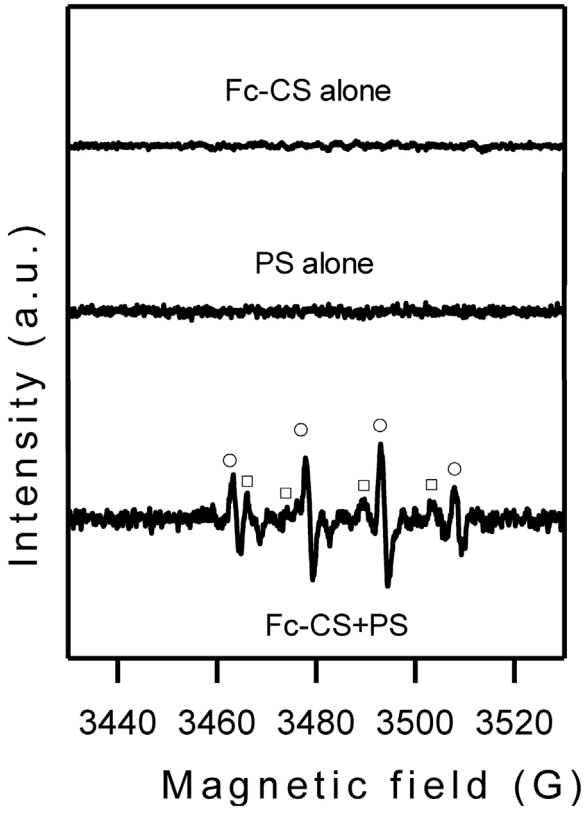

Fig. 8. EPR analyses of Fc-CS, PS, and Fc-CS + PS using DMPO as a radical trapping agent (○: DMPO—OH; □: DMPO-SO_4).

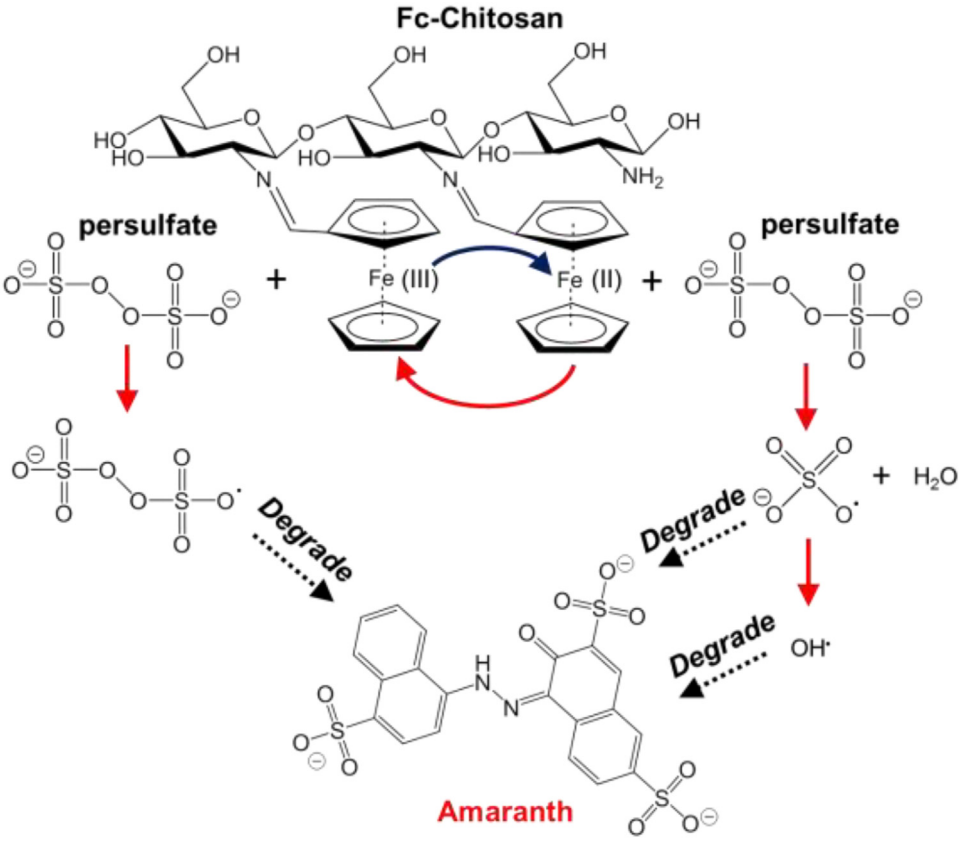

Fig. 9. Proposed mechanisms for PS activation by Fc-CS and AMR degradation by Fc-CS + PS.

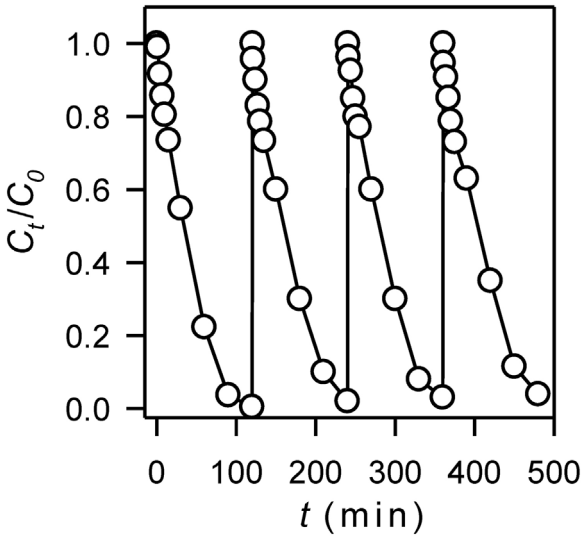

Fig. 10. Reusability of Fc-CS for activating PS to degrade AMR (Fc-CS = 250 mg L^{-1}; PS = 200 mg L^{-1}; T = 40 °C).

and then evolve into hydroxyl radicals (*i.e.*, $OH^{\bullet}$) via the follows reaction (Eq. (5)) (Xu, Chu, & Gan, 2015):

$$SO_4^{\bullet -} + H_2O \rightarrow SO_4^{2-} + OH^{\bullet} + H^+ \quad (5)$$

The EPR analysis demonstrates that AMR degradation can be attributed to both $SO_4^{\bullet -}$ and $OH^{\bullet}$. Based on these radicals, a possible mechanism is thus proposed as illustrated in Fig. 9. The catalytic transformation of Fe of Fc-CS activates PS for generation of $SO_4^{\bullet -}$ and $OH^{\bullet}$; $SO_4^{\bullet -}$ then induce the formation of $OH^{\bullet}$. These high-oxidation-potential radicals further attack AMR and cause decomposition.

3.7. *Recyclability of Fc-CS for activating PS to degrade AMR*

The recyclability of Fc-CS is one of the most critical aspects as a heterogeneous catalyst for PS activation. To evaluate the recyclability, Fc-CS was used over multiple times for activating PS for AMR degradation without any regeneration treatments. Fig. 10 shows a four-cycle AMR degradation by Fc-CS + PS, and the degradation extent and kinetics remained almost the same over the four cycles. Fig. S1(d) also displays the light absorption range of used Fc-CS, which was quite comparable with that of pristine Fc-CS, validating that Fc still remained on the CS surface and no significant color changes were observed. This demonstrates that Fc-CS can be a reusable and stable catalyst for activating PS. As Fc is anchored to CS, Fc-CS is also expected to be a more durable and robust heterogeneous catalyst for long-term applications.

4. Conclusions

In this study, CS was employed as a naturally polymeric support for immobilizing Fc. Fc was covalently bound to CS via the Schiff base reaction and therefore Fc was well dispersed on the CS surface without aggregation. As a result, the resulting Fc-CS exhibited a higher catalytic activity than pristine Fc for activating PS to degrade AMR. While the elevated temperatures and acidic conditions facilitated AMR degradation kinetics, the basic conditions suppressed the PS activation. In addition, the ionic surfactants also significantly influenced the AMR degradation. Through the EPR analysis, the AMR degradation can be attributed to both sulfate and hydroxyl radicals.

Fc-CS had been also proven to activate PS for AMR degradation over multiple times without loss of catalytic activity. These features indicate that Fc-CS can be a promising catalyst and CS appears to be a naturally available and environmentally friendly waste-derived support for immobilizing Fc. The results and findings in this study are essential for CS-supported metal catalysts in environmental applications.

Appendix A. Supplementary data

Supplementary data associated with this article can be found, in the online version, at 10.1016/j.carbpol.2017.06.015.

Reference:

Abdeen, Z., Mohammad, S. G., & Mahmoud, M. S. (2015). Adsorption of Mn (II) ion on polyvinyl alcohol/chitosan dry blending from aqueous solution. *Environmental Nanotechnology, Monitoring & Management*, *3*, 1–9.
Adil, M. R., Qadir, M. A., & Mahmood, K. (2009). Effects of various buffers and salt on color strength of reactive dye sumifix 3RF. *Journal of the Chemical Society of Pakistan*, *31*, 7–11.
Ahn, S., Peterson, T. D., Righter, J., Miles, D. M., & Tratnyek, P. G. (2013). Disinfection of ballast water with iron activated persulfate. *Environmental Science & Technology*, *47*, 11717–11725.
Cai, C., Zhang, Z., & Zhang, H. (2016). Electro-assisted heterogeneous activation of persulfate by Fe/SBA-15 for the degradation of Orange II. *Journal of Hazardous Materials*, *313*, 209–218.
Chen, Q., Xu, A., Li, Z., Wang, J., & Zhang, S. (2011). Influence of anionic structure on the dissolution of chitosan in 1-butyl-3-methylimidazolium-based ionic liquids. *Green Chemistry*, *13*, 3446–3452.
Chung, K. T., Fulk, G. E., & Egan, M. (1978). Reduction of azo dyes by intestinal anaerobes. *Applied and Environmental Microbiology*, *35*, 558–562.
Gao, Y.-q., Gao, N.-y., Deng, Y., Yang, Y.-q., & Ma, Y. (2012). Ultraviolet (UV) light-activated persulfate oxidation of sulfamethazine in water. *Chemical Engineering Journal*, *195–196*, 248–253.
Guo, W., Su, S., Yi, C., & Ma, Z. (2013). Degradation of antibiotics amoxicillin by Co3O4-catalyzed peroxymonosulfate system. *Environ Prog Sustain Energy*, *32*, 193–197.
Gupta, V. K., Jain, R., Mittal, A., Saleh, T. A., Nayak, A., Agarwal, S., et al. (2012). Photo-catalytic degradation of toxic dye amaranth on TiO2/UV in aqueous suspensions. *Materials Science and Engineering C*, *32*, 12–17.
Hu, P., & Long, M. (2016). Cobalt-catalyzed sulfate radical-based advanced oxidation: A review on heterogeneous catalysts and applications. *Applied Catalysis B*, *181*, 103–117.
Huang, K.-C., Couttenye, R. A., & Hoag, G. E. (2002). Kinetics of heat-assisted persulfate oxidation of methyl tert-butyl ether (MTBE). *Chemosphere*, *49*, 413–420.
Khan, N. A., & Jhung, S. H. (2009). Facile syntheses of metal-organic framework Cu3(BTC)2(H2O)3 under ultrasound. *Bulletin of the Korean Chemical Society*, *30*, 2921–2926.
Kiener, M.A. (1991). Chemical cleaning solution and method. Google Patents.
King, J.J. (1983). Inorganic persulfate cleaning solution for acoustic materials. Google Patents.
Kurukutla, A. B., Kumar, P. S. S., Anandan, S., & Sivasankar, T. (2014). Sonochemical degradation of rhodamine B using oxidants, hydrogen Peroxide/Peroxydisulfate/Peroxymonosulfate, with Fe2+ ion: Proposed pathway and kinetics. *Environmental Engineering Science*, *32*, 129–140.
Li, Y., Xue, L., Li, H., Li, Z., Xu, B., Wen, S., et al. (2009). Energy level and molecular structure engineering of conjugated donor-Acceptor copolymers for photovoltaic applications. *Macromolecules*, *42*, 4491–4499.
Liang, C., Bruell, C. J., Marley, M. C., & Sperry, K. L. (2004). Persulfate oxidation for in situ remediation of TCE. I. Activated by ferrous ion with and without a persulfate–thiosulfate redox couple. *Chemosphere*, *55*, 1213–1223.
Liang, C., Liang, C.-P., & Chen, C.-C. (2009). pH dependence of persulfate activation by EDTA/Fe(III) for degradation of trichloroethylene. *Journal of Contaminant Hydrology*, *106*, 173–182.
Liao, Q., Sun, J., & Gao, L. (2009). Degradation of phenol by heterogeneous Fenton reaction using multi-walled carbon nanotube supported Fe2O3 catalysts. *Colloids and Surfaces A: Physicochemical and Engineering Aspects*, *345*, 95–100.
Lin, K.-Y. A., Chang, H.-A., & Hsu, C.-J. (2015). Iron-based metal organic framework, MIL-88A, as a heterogeneous persulfate catalyst for decolorization of rhodamine B in water. *RSC Advances*, *5*, 32520–32530.
Lin, K.-Y. A., Lin, J.-T., & Jochems, A. P. (2017). Oxidation of amaranth dye by persulfate and peroxymonosulfate activated by ferrocene. *Journal of Chemical Technology & Biotechnology*, *92*, 163–172.
Liu, J., Zhang, T., Wang, Z., Dawson, G., & Chen, W. (2011). Simple pyrolysis of urea into graphitic carbon nitride with recyclable adsorption and photocatalytic activity. *Journal of Materials Chemistry*, *21*, 14398–14401.
Liu, C. S., Shih, K., Sun, C. X., & Wang, F. (2012). Oxidative degradation of propachlor by ferrous and copper ion activated persulfate. *Science of The Total Environment*, *416*, 507–512.
Liu, H., Bruton, T. A., Doyle, F. M., & Sedlak, D. L. (2014). In situ chemical oxidation of contaminated groundwater by persulfate: Decomposition by Fe(III)- and

Mn(IV)-containing oxides and aquifer materials. *Environmental Science & Technology*, *48*, 10330–10336.
Liu, H., Bruton, T. A., Li, W., Buren, J. V., Prasse, C., Doyle, F. M., et al. (2016). Oxidation of benzene by persulfate in the presence of Fe(III)- and Mn(IV)-containing oxides: Stoichiometric efficiency and transformation products. *Environmental Science & Technology*, *50*, 890–898.
Lu, Y.-S., Wang, Z., Xu, Y.-F., Liu, Q., & Qian, G.-R. (2016). Fe2(MoO4)3 as a novel heterogeneous catalyst to activate persulfate for Rhodamine B degradation. *Desalination and Water Treatment*, *57*, 7898–7909.
Matzek, L. W., & Carter, K. E. (2016). Activated persulfate for organic chemical degradation: A review. *Chemosphere*, *151*, 178–188.
McElroy, W. J., & Waygood, S. J. (1990). Kinetics of the reactions of the SO radical with SO, S2O, H2O and Fe2+. *Journal of the Chemical Society, Faraday Transactions*, *86*, 2557–2564.
Mittal, A., Kurup, L., & Gupta, V. K. (2005). Use of waste materials—Bottom ash and de-oiled soya, as potential adsorbents for the removal of Amaranth from aqueous solutions. *Journal of Hazardous Materials*, *117*, 171–178.
Muthukumar, M., Sargunamani, D., Selvakumar, N., & Nedumaran, D. (2004). Effect of salt additives on decolouration of Acid Black 1 dye effluent by ozonation. *Indian Journal of Chemical Technology*, *11*, 612–616.
Neta, P., Huie, R. E., & Ross, A. B. (1988). Rate constants for reactions of inorganic radicals in aqueous solution. *Journal of Physical and Chemical Reference Data*, *17*, 1027–1284.
Nie, Y., Hu, C., Qu, J., & Hu, X. (2008). Efficient photodegradation of Acid Red B by immobilized ferrocene in the presence of UVA and H2O2. *Journal of Hazardous Materials*, *154*, 146–152.
Qi, F., Chu, W., & Xu, B. (2014). Modeling the heterogeneous peroxymonosulfate/Co-MCM41 process for the degradation of caffeine and the study of influence of cobalt sources. *Chemical Engineering Journal*, *235*, 10–18.
Rastogi, A., Al-Abed, S. R., & Dionysiou, D. D. (2009). Sulfate radical-based ferrous–peroxymonosulfate oxidative system for PCBs degradation in aqueous and sediment systems. *Applied Catalysis B: Environmental*, *85*, 171–179.
Rodriguez, S., Vasquez, L., Costa, D., Romero, A., & Santos, A. (2014). Oxidation of Orange G by persulfate activated by Fe(II), Fe(III) and zero valent iron (ZVI). *Chemosphere*, *101*, 86–92.
Sudrajat, H., & Babel, S. (2015). Rapid photocatalytic degradation of the recalcitrant dye amaranth by highly active N-WO3. *Environmental Chemistry Letters*, 1–7.
Tsai, F.-C., Chang, C.-C., Liu, C.-L., Chen, W.-C., & Jenekhe, S. A. (2005). New thiophene-linked conjugated poly(azomethine)s: Theoretical electronic structure, synthesis, and properties. *Macromolecules*, *38*, 1958–1966.
Wang, Q., Tian, S., Cun, J., & Ning, P. (2013). Degradation of methylene blue using a heterogeneous Fenton process catalyzed by ferrocene. *Desalination Water Treatment*, *51*, 5821–5830.
Weng, C.-H., Tao, H., Highly efficient persulfate oxidation process activated with Fe0 aggregate for decolorization of reactive azo dye Remazol Golden Yellow. *Arabian Journal of Chemistry*, https://doi.org/10.1016/j.arabjc.2015.05.012.
Wu, Y., Prulho, R., Brigante, M., Dong, W., Hanna, K., & Mailhot, G. (2017). Activation of persulfate by Fe(III) species: Implications for 4-tert-butylphenol degradation. *Journal of Hazardous Materials*, *322*(Part B), 380–386.
Xiang, J., Yang, X., Chen, C., Tang, Y., Yan, W., & Xu, G. (2003). Effects of NaCl on the J-aggregation of two thiacarbocyanine dyes in aqueous solutions. *Journal of Colloid and Interface Science*, *258*, 198–205.
Xu, L. J., Chu, W., & Gan, L. (2015). Environmental application of graphene-based CoFe2O4 as an activator of peroxymonosulfate for the degradation of a plasticizer. *Chemical Engineering Journal*, *263*, 435–443.
Yang, S., Wang, P., Yang, X., Shan, L., Zhang, W., Shao, X., et al. (2010). Degradation efficiencies of azo dye Acid Orange 7 by the interaction of heat, UV and anions with common oxidants: Persulfate, peroxymonosulfate and hydrogen peroxide. *Journal of Hazardous Materials*, *179*, 552–558.
Ye, X., Cui, Y., & Wang, X. (2014). Ferrocene-modified carbon nitride for direct oxidation of benzene to phenol with visible light. *ChemSusChem*, *7*, 738–742.
Ye, X., Zheng, Y., & Wang, X. (2014). Synthesis of ferrocene-Modified carbon nitride photocatalysts by surface amidation reaction for phenol synthesis. *Chinese Journal of Chemistry*, *32*, 498–506.
Yin, P., Hu, Z., Song, X., Liu, J., & Lin, N. (2016). Activated persulfate oxidation of perfluorooctanoic acid (PFOA) in groundwater under acidic conditions. *International Journal of Environmental Research and Public Health*, *13*, 602.
Yu, X.-Y., Bao, Z.-C., & Barker, J. R. (2003). Free radical reactions involving cl•, cl2-•, and SO4-• in the 248 nm photolysis of aqueous solutions containing S2O82- and Cl. *The Journal of Physical Chemistry A*, *108*, 295–308.
Zeng, H., Liu, S., Chai, B., Cao, D., Wang, Y., & Zhao, X. (2016). Enhanced photoelectrocatalytic decomplexation of Cu–EDTA and Cu recovery by persulfate activated by UV and cathodic reduction. *Environmental Science & Technology*, *50*, 6459–6466.
Zhang, J., Chen, M., & Zhu, L. (2016). Activation of persulfate by Co3O4 nanoparticles for orange G degradation. *RSC Advances*, *6*, 758–768.
Zhao, X., Yeung, C. S., & Dong, V. M. (2010). Palladium-catalyzed ortho-arylation of O-phenylcarbamates with simple arenes and sodium persulfate. *Journal of the American Chemical Society*, *132*, 5837–5844.
Zhao, D., Liao, X., Yan, X., Huling, S. G., Chai, T., & Tao, H. (2013). Effect and mechanism of persulfate activated by different methods for PAHs removal in soil. *Journal of Hazardous Materials*, *254–255*, 228–235.